

## Research Article

# An Experimental Study of the Formation of Talc through $\text{CaMg}(\text{CO}_3)_2\text{-SiO}_2\text{-H}_2\text{O}$ Interaction at 100–200°C and Vapor-Saturation Pressures

Ye Wan,<sup>1</sup> Xiaolin Wang,<sup>1,2,3</sup> I-Ming Chou,<sup>4</sup> Wenxuan Hu,<sup>1,2</sup>  
Yang Zhang,<sup>1</sup> and Xiaoyu Wang<sup>1</sup>

<sup>1</sup>State Key Laboratory for Mineral Deposits Research, School of Earth Sciences and Engineering, Nanjing University, Nanjing, Jiangsu 210023, China

<sup>2</sup>Institute of Energy Sciences, Nanjing University, Nanjing, Jiangsu 210023, China

<sup>3</sup>Shandong Provincial Key Laboratory of Depositional Mineralization and Sedimentary Minerals, Shandong University of Science and Technology, Qingdao, Shandong 266510, China

<sup>4</sup>Laboratory of Experimental Study under Deep-Sea Extreme Conditions, Institute of Deep-Sea Science and Engineering, Chinese Academy of Sciences, Sanya, Hainan 572000, China

Correspondence should be addressed to Xiaolin Wang; [xlinwang@nju.edu.cn](mailto:xlinwang@nju.edu.cn) and Wenxuan Hu; [huwx@nju.edu.cn](mailto:huwx@nju.edu.cn)

Received 14 February 2017; Accepted 31 May 2017; Published 4 July 2017

Academic Editor: Daniel E. Harlov

Copyright © 2017 Ye Wan et al. This is an open access article distributed under the Creative Commons Attribution License, which permits unrestricted use, distribution, and reproduction in any medium, provided the original work is properly cited.

The metamorphic interaction between carbonate and silica-rich fluid is common in geological environments. The formation of talc from dolomite and silica-rich fluid occurs at low temperatures in the metamorphism of the  $\text{CaO-MgO-SiO}_2\text{-CO}_2\text{-H}_2\text{O}$  system and plays important roles in the formation of economically viable talc deposits, the modification of dolomite reservoirs, and other geological processes. However, disagreement remains over the conditions of talc formation at low temperatures. In this study, in situ Raman spectroscopy, quenched scanning electron microscopy, micro-X-ray diffraction, and thermodynamic calculations were used to explore the interplay between dolomite and silica-rich fluids at relatively low temperatures in fused silica tubes. Results showed that talc formed at  $\leq 200^\circ\text{C}$  and low  $\text{CO}_2$  partial pressures ( $PCO_2$ ). The reaction rate increased with increasing temperature and decreased with increasing  $PCO_2$ . The major contributions of this study are as follows: (1) we confirmed the formation mechanism of Mg-carbonate-hosted talc deposits and proved that talc can form at  $\leq 200^\circ\text{C}$ ; (2) the presence of talc in carbonate reservoirs can indicate the activity of silica-rich hydrothermal fluids; and (3) the reactivity and solubility of silica require further consideration, when a fused silica tube is used as the reactor in high  $P$ - $T$  experiments.

## 1. Introduction

The common metamorphic interaction between dolomite and silica-rich fluids plays important roles in many geological processes. For example, the interaction is closely associated with the formation of skarn ore deposits [1–3]. Talc was reported to form at low temperatures in the metamorphism of the  $\text{CaO-MgO-SiO}_2\text{-H}_2\text{O-CO}_2$  system [4–6]. Talc is characterized by a trioctahedron structure [7] and is chemically inert, soft, white, and highly thermally conductive [8]. As a result, talc is used in various industrial applications [7, 9, 10]. Previous studies showed that talc mineralization can occur in various geological settings, such as the alteration

of ultra-mafic rocks (e.g., [11–15]), the mixing of seafloor hydrothermal fluids and seawater [16], and the alteration of Mg-carbonate rocks [17–21]. However, it is most economical to extract from deposits associated with the hydrothermal alteration of dolostone/Mg-carbonate [17].

Hydrothermal dolomite and hydrothermally altered dolomite are important hydrocarbon reservoirs (e.g., [22–25]). Geologically pervasive silica-rich hydrothermal fluids derived from sources, such as deep formation brines or magma intrusions (e.g., [26–28]), can react with dolomite to form talc in carbonate reservoirs, influencing the reservoirs' physical properties [29–31]. In addition, talc has

a low friction coefficient, so its formation along faults in carbonate rocks can promote the stable creep of a fault, releasing accumulated elastic strain and preventing strong earthquakes [32–35]. Therefore, thorough investigation of the  $\text{CaMg}(\text{CO}_3)_2\text{-SiO}_2\text{-H}_2\text{O}$  interaction can help elucidate many geological processes.

However, disagreements remained regarding the formation temperature of talc through the reaction between dolomite and a silica-rich fluid. The reaction has been theoretically calculated to occur at  $\geq 150^\circ\text{C}$  [5, 35, 36], but most geological studies have indicated that talc mainly forms at  $250\text{--}400^\circ\text{C}$  (e.g., [21, 37, 38]). For example, in the Saint-Barthélemy deposits in Switzerland, oxygen isotope thermometric calculations showed that talc mineralization occurred at about  $300^\circ\text{C}$  [21], which is consistent with fluid inclusion data ( $250\text{--}300^\circ\text{C}$ ) [39, 40]. Experimental studies have sought to construct a phase diagram of the  $\text{CaO-MgO-SiO}_2\text{-CO}_2\text{-H}_2\text{O}$  system, but hydrothermal experimental studies have only been conducted above  $250^\circ\text{C}$  (e.g., [4, 41–44]). Consequently, further experiments at lower temperatures are necessary to fully explore the formation temperature of talc.

In this study, the reactions for the  $\text{CaMg}(\text{CO}_3)_2\text{-SiO}_2\text{-H}_2\text{O}$  system were conducted in fused silica tubes at temperatures from  $100$  to  $200^\circ\text{C}$ . In situ Raman spectroscopy was used to characterize the vapor products. The quenched solid products were investigated with Raman spectroscopy, scanning electron microscopy (SEM) equipped with an energy dispersive spectrometer (EDS), and micro-X-ray diffraction (micro-XRD). In addition, the Gibbs free energy of the reaction was also calculated using the geochemical modelling program.

## 2. Materials and Methods

**2.1. Sample Preparation.** Dolomite powder was prepared from dolomite rocks of the Neoproterozoic Dengying Formation in the Sichuan Basin, Southwest China. Powder XRD analyses showed that the dolomite rock is comprised of  $>97\%$  dolomite and  $<3\%$  quartz. Calcite grains were prepared from colorless, transparent, rhombohedral calcite crystals. Distilled deionized water ( $18.2\text{ K}\Omega\cdot\text{cm}$ ) was used throughout. Amorphous  $\text{SiO}_2$  originated from the fused silica tubes.

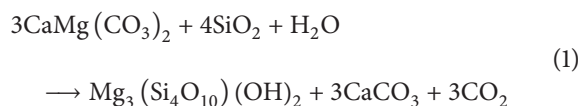
Chou et al. [46] have reported detailed procedures for constructing fused silica capillary capsules (FSCCs). The protective polyimide layer of the fused silica tube ( $0.5\text{ mm}$  in inner diameter and  $0.65\text{ mm}$  in outer diameter) was burnt off in an oxyhydrogen flame, and one end of the tube was sealed. The dolomite/calcite powder and a  $0.5\text{-cm}$  long water column were loaded into the tube and centrifuged to the sealed end. The open end was then connected to a pressure line. The air in the tube was evacuated, and the open end of the tube was sealed by fusion in the oxyhydrogen flame. As shown in Figure 1, the prepared FSCC is about  $2\text{ cm}$  long and consists of the dolomite powder ( $\sim 0.5\text{ cm}$  in length), water ( $\sim 0.5\text{ cm}$  in length), and a vapor phase ( $\sim 1\text{ cm}$  in length).

High-pressure optical cells (HPOCs, Figure 2(a)) containing dolomite and water were also constructed for pressure

measurements. The dolomite powder and deionized water were first loaded into a one-end-sealed fused silica tube ( $\sim 20\text{ cm}$  in length). Approximately  $2\text{ cm}$  long mercury was then injected to separate the reaction system and the pressurization medium—water. The detailed procedures for preparing HPOCs are described in Chou et al. [47].

### 2.2. Experimental Procedures

**2.2.1. In Situ Vapor-Phase Analyses.** The reaction between dolomite and a silica-rich fluid to form talc involves decarbonation of dolomite and the generation of  $\text{CO}_2$ :



Raman spectroscopy is sensitive to  $\text{CO}_2$  and can detect  $\text{CO}_2$  at pressures lower than  $0.6\text{ bar}$  [48, 49]. Therefore, in situ Raman spectroscopy of the vapor phase was used to detect the reaction. FSCCs containing dolomite and water were heated in a heating stage (Linkam CAP500) calibrated with a K-type thermocouple, which had been previously calibrated with the triple point ( $0^\circ\text{C}$ ) and boiling point ( $100^\circ\text{C}$ ) of water at  $0.1\text{ MPa}$ . The temperature difference along the  $4\text{ cm}$  central line of the heating stage was less than  $0.5^\circ\text{C}$  at  $300^\circ\text{C}$ . The setup of in situ Raman spectroscopic analysis is shown in Figure 1. The target temperature was increased at increments of  $10^\circ\text{C}$  from an initial  $60^\circ\text{C}$ , until a  $\text{CO}_2$  signal was detected in the vapor phase after heating for  $\sim 24\text{ h}$ . To characterize the mechanism of  $\text{CO}_2$  generation (metamorphic alteration or decomposition of dissolved  $\text{CO}_3^{2-}$ ), Raman spectra of the vapor phase within FSCCs containing calcite and water were also acquired for comparison.

Raman spectra were collected in situ for the vapor phase within FSCCs containing dolomite and water at  $200^\circ\text{C}$  (higher than the reaction threshold) to investigate the kinetics of the reaction. The experimental duration was increased from  $2\text{ h}$  to  $\sim 240\text{ h}$ .

**2.2.2. Pressure Measurements.** The setup for the pressure measurement is shown in Figure 2(a). The HPOC containing dolomite and water was connected to a pressurization system. Pressures were monitored by a Setra 206D digital pressure transducer with Datum 2002 manometer ( $69\text{ MPa}$  full scale, accurate to  $\pm 0.14\%$ ). The HPOC containing dolomite and water was heated to  $200^\circ\text{C}$  using a Linkam CAP 500 heating stage. The position of mercury in the HPOC was fixed by adjusting the pressure with a pressure generator, and then the pressure of the whole system was recorded with experimental duration (Figure 2(a)).

**2.2.3. Analyses of Solid Products.** Several one-end-open fused silica tubes containing dolomite and water were placed in a  $10\text{ mL}$  batch stainless steel reactor equipped with a Teflon (PTFE) internal cup (Figure 2(b)). The reactor was then heated at  $150$  and  $200^\circ\text{C}$  for  $20\text{--}90$  days in an oven with a temperature accuracy of  $\pm 5^\circ\text{C}$ . During the reaction, the reactor was opened and the product  $\text{CO}_2$  was released several

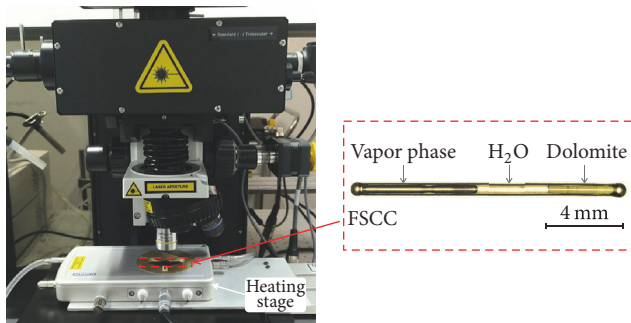


FIGURE 1: Setup for in situ analyses of the vapor phase within a FSCC containing dolomite and water.

times to promote the reaction. After heating, micro-XRD and Raman spectroscopy were used to characterize the composition of the quenched solid product at room temperature. Then, the SEM was used to observe the morphology of the product. The chemical composition was analyzed using EDS.

**2.3. Analytical Methods.** Raman spectra were collected with a high-resolution Raman spectrometer (LabRAM HR800, JY/Horiba) using a 532.11 nm laser from an air-cooled, frequency-doubled Nd:YAG laser excitation, a 50x objective (Olympus), and a 1800 groove/mm grating with a spectral resolution of about  $1 \text{ cm}^{-1}$ . An approximate 9.5 mW laser was focused on the central level of the horizontal tube for vapor spectra acquisition and on the surface of the solid phase for solid spectra acquisition. Spectra were collected from 100 to  $1600 \text{ cm}^{-1}$ . To obtain a high signal-to-noise ratio spectrum, three accumulations were collected in denoise mode (120 s for the vapor phase and 30 s for the solid phase), and averaged for each spectrum. Before collection, the Raman spectrometer was calibrated with the  $\nu_1$  band of silicon at  $520.2 \text{ cm}^{-1}$  [50]. Labspec 5 software was used for Raman spectral analyses.

Micro-XRD investigations of the quenched reacted dolomite were carried out with a diffractometer (D/max Rapid II, Rigaku) equipped with a Mo tube and a  $300\text{-}\mu\text{m}$  diameter collimator. The diffractometer was operated at 50 kV and 90 mA with an angular velocity of  $6^\circ/\text{s}$  and an exposure time of 15 min. Jade 6 software was used to characterize the compositions of the solid phase.

The morphology of the quenched reacted dolomite was observed using a field emission (FE) SEM (Supra55, Zeiss) with an accelerating voltage of 15 kV. The approximate chemical composition of the solid phase was analyzed by an EDS (Oxford Instruments, Inca X-Max 150  $\text{mm}^2$ ). All experiments were performed at the Institute of Energy Sciences and the State Key Laboratory for Mineral Deposits Research hosted in School of Earth Sciences and Engineering, Nanjing University.

In addition, we calculated the Gibbs free energy of talc formation from the  $\text{CaMg}(\text{CO}_3)_2\text{-SiO}_2(\text{aq})\text{-H}_2\text{O}$  system for the  $P\text{-}T$  conditions covered in these experiments, using the Hch program (version 4.4) and its incorporated Unitherm database [51].

### 3. Results

**3.1. Vapor-Phase Characterization.** The linear  $\text{CO}_2$  molecule has four vibrational modes: a symmetric stretching mode ( $\nu_1$ ), two bending modes ( $2\nu_2$ :  $\nu_{2a}$  and  $\nu_{2b}$ ), and an antisymmetric stretching mode ( $\nu_3$ ) (e.g., [48, 52, 53]). The modes  $\nu_1$  and  $2\nu_2$  are both Raman active and have a similar energy ( $\sim 1335 \text{ cm}^{-1}$ ) and the same symmetry species, resulting in a Fermi resonance [48]. Fermi resonance causes the excited admixed states to split into two prominent peaks: an upper band at  $\sim 1388 \text{ cm}^{-1}$  and a lower band at  $\sim 1285 \text{ cm}^{-1}$  [48, 54]. Weak hot bands flanking the Fermi diads may also appear in the spectrum [48]. Raman spectroscopy has very low detection limits for  $\text{CO}_2$  and thus is used frequently for  $\text{CO}_2$  characterization in fluid inclusions [53, 55–58].

Figure 3(a) shows the Raman spectra of the vapor phase in FSCCs containing  $\text{CaMg}(\text{CO}_3)_2\text{-H}_2\text{O}$  and  $\text{CaCO}_3\text{-H}_2\text{O}$  after heating at  $90\text{--}150^\circ\text{C}$  for 24 h. For the FSCCs containing dolomite and water, no  $\text{CO}_2$  signal was observed after heating at  $\leq 90^\circ\text{C}$ . Weak but clear  $\text{CO}_2$  Fermi bands at  $\sim 1285$  and  $1384 \text{ cm}^{-1}$  were observed after heating at  $100^\circ\text{C}$ . The Raman intensity of  $\text{CO}_2$  was much stronger after heating at  $150^\circ\text{C}$  than that at  $100^\circ\text{C}$  (Figure 3(a)). That is to say,  $\text{CO}_2$  was generated in the  $\text{CaMg}(\text{CO}_3)_2\text{-SiO}_2\text{-H}_2\text{O}$  system when heated at  $\geq 100^\circ\text{C}$  with an experimental duration of 24 h. However, the signals of  $\text{CO}_2$  were not observed in FSCCs containing calcite and water after heating at  $100\text{--}200^\circ\text{C}$  for 24 h. Considering that a greater concentration of  $\text{CO}_3^{2-}$  dissolved from calcite than from dolomite in pure water at temperatures of  $100\text{--}150^\circ\text{C}$  [59, 60], we suggest that the  $\text{CO}_2$  from the dolomite-bearing system was generated by decarbonation via metamorphic reaction (1) instead of the decomposition of dissolved  $\text{CO}_3^{2-}$ .

The intensity and wavenumber of the  $\text{CO}_2$  Fermi diad bands vary with changes in the  $\text{CO}_2$  pressure and temperature [48, 53, 56]. Previous studies have suggested that the Fermi diad splits increase with increasing  $\text{CO}_2$  pressure at a constant temperature (e.g., [61]). Accordingly, several equations were constructed for quantitative measurements of the  $\text{CO}_2$  density based on the Fermi diad splits by using reference samples with  $P_{\text{CO}_2} > 0.6 \text{ bar}$  ([49] and references therein). In this study, the Fermi diad peak positions and splits of  $\text{CO}_2$  produced from  $\text{CaMg}(\text{CO}_3)_2\text{-SiO}_2\text{-H}_2\text{O}$  interaction were also obtained (Table 1). However, negative density values were obtained when applying these calibration curves to quantitatively measure the  $\text{CO}_2$  content in the FSCC. This result indicates that only a small amount of  $\text{CO}_2$  was produced in the FSCC and that the  $\text{CO}_2$  pressure was lower than 0.6 bar. Table 2 shows the variation of the internal pressure of a HPOC containing dolomite and water with experimental duration. Results showed that the internal pressure fluctuated with reaction time. Consequently, the exact partial pressure of  $\text{CO}_2$  generated from the metamorphic reaction (1) cannot be obtained; this should also result from the very low  $P_{\text{CO}_2}$ .

The variation in the Raman intensity of  $\text{CO}_2$  as a function of the experimental duration can reflect the kinetics of reactions yielding  $\text{CO}_2$  [57]. Increasing the experimental duration could increase the  $\text{CO}_2$  intensity (Figure 3(b)). The peak areas

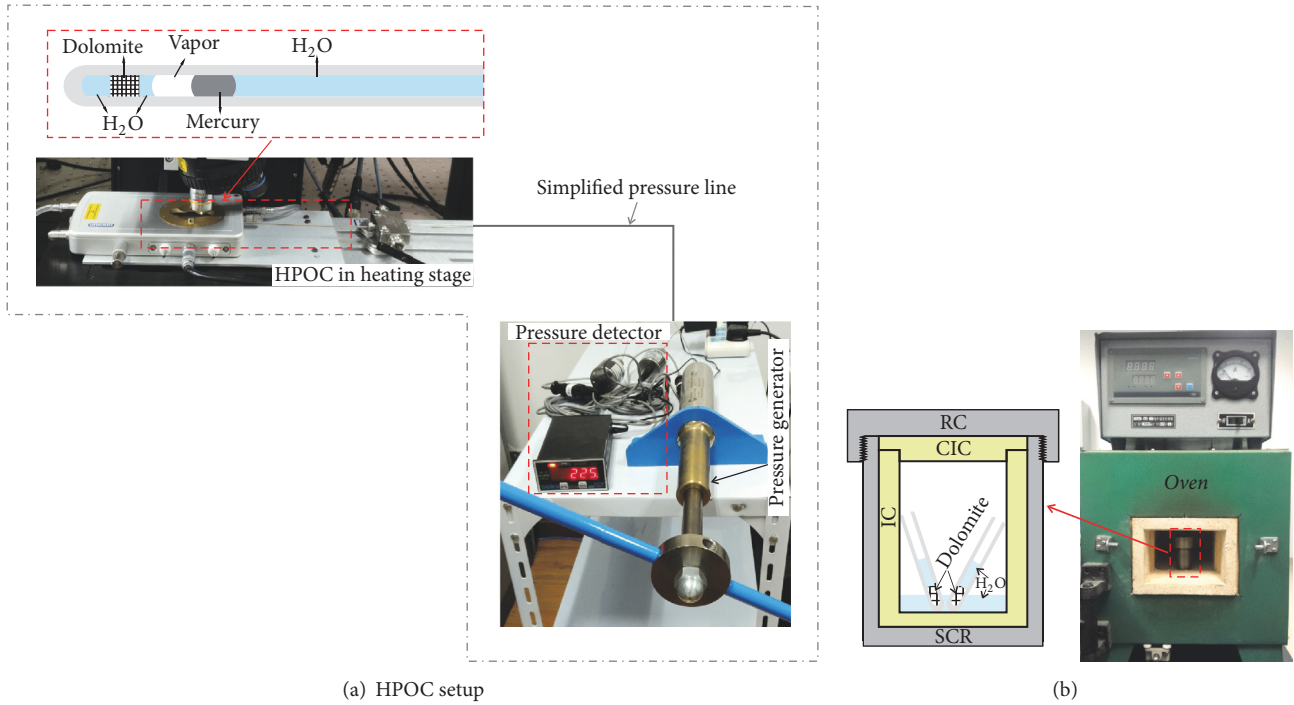


FIGURE 2: (a) The setup for measurements of the internal pressures within a HPOC containing dolomite and water; (b) the batch stainless reactor in the oven. The left schematic diagram showing the structure of the reactor. SCR represents the stainless cup of the reactor, RC represents the reactor cover, IC represents internal cup, and CIC represents cover of the internal cup.

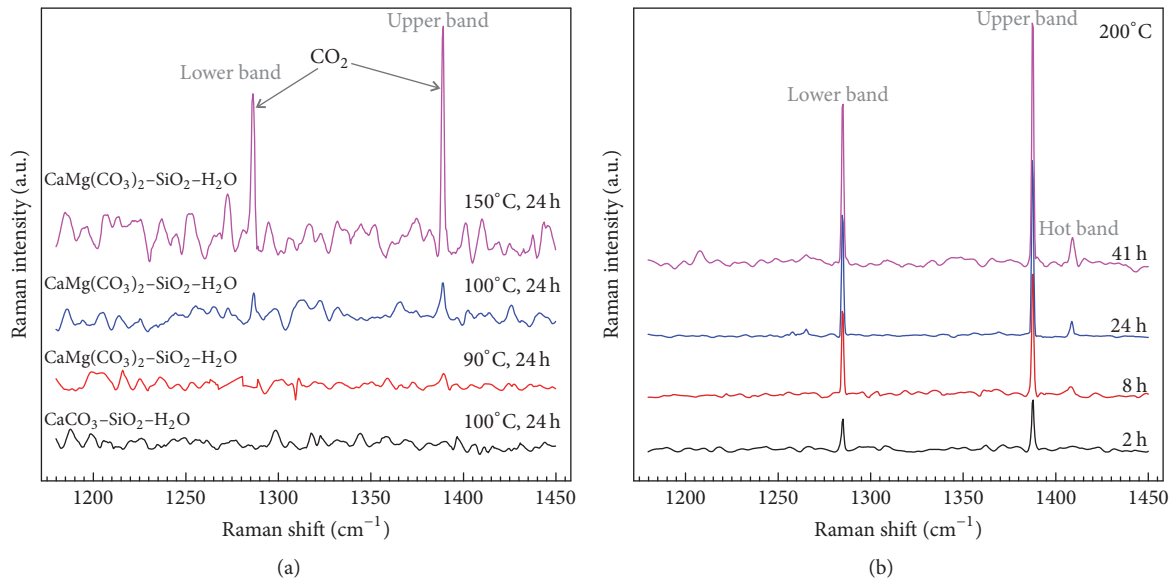


FIGURE 3: Raman spectra of the vapor phase in FSCCs containing (a)  $\text{CaCO}_3\text{-H}_2\text{O}$  and  $\text{CaMg}(\text{CO}_3)_2\text{-H}_2\text{O}$  after heating at 90–150°C for 24 h and (b)  $\text{CaMg}(\text{CO}_3)_2\text{-H}_2\text{O}$  after heating at 200°C from 2 to 41 h.

of the  $\text{CO}_2$  Fermi diad bands increased with experimental duration up to about 120 h (200°C) before eventually leveling off (Figure 4, Table 1). Solid-phase characterization (see Section 3.2) indicated that the dolomite was unlikely to run out over the length of the experiment. Consequently, the reaction reached an equilibrium state after reaction for ~120 h. The degree of the reaction ( $R$ ) can be calculated using

the ratio between the total Raman peak area of  $\text{CO}_2$  at time  $t$  ( $A$ ) and that at equilibrium state ( $A^*$ ):

$$R(\%) = \frac{A}{A^*} \times 100\%. \quad (2)$$

As shown in Figure 4 (diamonds), the slope of  $R$  decreases with the increase of reaction time, indicating that the

TABLE 1: Fermi diad bands, splits, and peak areas of CO<sub>2</sub> generated in the FSCC containing dolomite and water at 200°C, and the calculated degree of reaction.

Reaction time (h)	Fermi diads and splits (cm <sup>-1</sup> )			Peak area			Degree of reaction (%) <sup>a</sup>
	$\nu_1$	$\nu_2$	$\Delta$	$\nu_1$	$\nu_2$	$\nu_1 + \nu_2$	
0	—	—	—	0	0	0	0
2	1285.21	1387.92	102.71	315.87	366.62	682.49	15.8
4	1285.19	1387.77	102.58	530.83	775.21	1306.04	30.2
6	1285.09	1387.7	102.61	551.64	817.14	1368.78	31.6
8	1285.14	1387.72	102.58	599.66	955	1554.66	35.9
10	1284.84	1387.49	102.65	731.41	1023.21	1754.62	40.6
20	1285.51	1388.04	102.53	900.65	1419.02	2319.67	53.6
22	1285.45	1388	102.55	1000.18	1483.36	2483.54	57.4
28	1285.37	1387.95	102.58	1155.19	1718.56	2873.75	66.4
40	1285.43	1387.98	102.55	1327.9	1910.84	3238.74	74.8
43	1285.66	1388.21	102.55	1270.99	1887.07	3158.06	73.0
46	1285.76	1388.23	102.47	1388.06	1995.8	3383.86	78.2
49	1285.63	1388.17	102.54	1346.42	1921.19	3267.61	75.5
60	1285.39	1387.94	102.55	1370.6	2163.74	3534.34	81.7
65	1285.62	1388.16	102.54	1433.07	2208.62	3641.69	84.2
70	1285.59	1388.14	102.55	1454.65	2172.31	3626.96	83.8
87	1285.01	1387.57	102.56	1561.79	2307.84	3869.63	89.4
92	1285.49	1387.93	102.44	1623.26	2288.82	3912.08	90.4
104	1285.73	1388.11	102.38	1713.6	2457.37	4170.97	96.4
137	1285.67	1388.04	102.37	1729.76	2589.05	4318.81	
149	1285.26	1387.99	102.73	1746.57	2501.63	4248.2	
159	1285.38	1387.97	102.59	1836.27	2553.95	4390.22	
171	1285.31	1387.93	102.62	1797.81	2599.46	4397.27	
193	1285.24	1387.77	102.53	1697.12	2681.04	4378.16	
203	1285.37	1387.95	102.58	1755.2	2555.08	4310.28	
213	1285.66	1388.21	102.55	1740.85	2548.89	4289.74	
224	1285.6	1388.15	102.55	1725	2559.7	4284.7	

<sup>a</sup>The total Raman peak area of CO<sub>2</sub> at equilibrium state is an average of those after reaction for ~120 h. Then, the degree of reaction can be regarded as 100% when the reaction time exceeds 120 h.

reaction rates decrease with the increase of experimental duration/ $PCO_2$ . The results also showed that the reaction rate increased with increasing temperature. For example, the Raman intensity of CO<sub>2</sub> was stronger at higher temperature within a given period of time (Figure 3(a)).

**3.2. Solid-Phase Characterization.** Figure 5 shows XRD patterns of the quenched solid relicts in the fused silica tubes. After heating at 200°C for ~20 days, the talc signals were weak. However, heating for 80 days produced calcite and talc as the main phases in the solid relicts, whereas dolomite signals were hardly visible in the XRD pattern (Figure 5).

The Raman spectrum of the solid phase before heating (Figure 6) showed only dolomite peaks (~177, 300.5, 1098 cm<sup>-1</sup>; [62]), indicating that the dolomite was of high purity, consistent with the XRD analysis. However, in addition to dolomite, characteristic calcite signals (~282 and 1086 cm<sup>-1</sup>; [63]) and talc signals (190.5, 360.5, and 675 cm<sup>-1</sup>; [64]) appeared after heating at 200°C for 60 days.

Figure 7 shows the morphology of the solid phase after heating at 200°C for 60 days. The solid phase has a honeycomb-like texture and was widely distributed in the relicts (Figures 7(a)–7(d)). It was identified by EDS as talc (Figure 7(c)). The talc exhibited unoriented textures because it formed under strain-free conditions [21]. Some cylindrical talc also occurred along the inner surface of the FSCC (Figure 7(d)). The dolomite grains had smooth edges (Figure 7(c)), indicating dissolution during heating. Some products of rhombohedral calcite (Figure 7(d)) were also present in the solid phase, which formed along with the talc via reaction (1).

The amount of Mg-silicate mineral produced at 150°C for 40 days was below the detection limit of the micro-XRD equipment. Only dolomite and a small amount of calcite were observed in the XRD pattern after heating at 150°C for 40 days (Figure 5). This further supports the view that the metamorphic reaction rate is largely dependent on temperature. Some researchers view talc as the initial metamorphic mineral for the CaMg(CO<sub>3</sub>)<sub>2</sub>-SiO<sub>2</sub>-H<sub>2</sub>O system

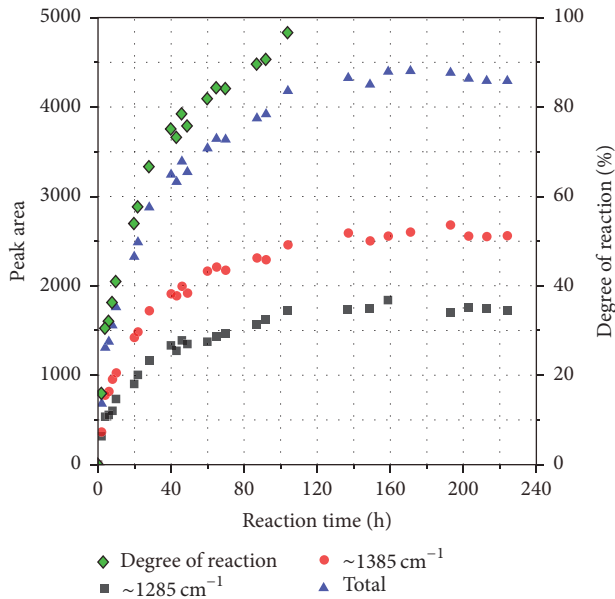


FIGURE 4: Raman peak areas of  $\text{CO}_2$  and the degree of reaction versus reaction time at  $200^\circ\text{C}$ . Black rectangles and red circles denote the peak areas of the lower band at  $\sim 1285\text{ cm}^{-1}$  and the upper band at  $\sim 1385\text{ cm}^{-1}$ , respectively. Blue triangles represent the total peak areas of both bands. The green diamonds represent the degree of the reaction. Data plotted are from Table 1.

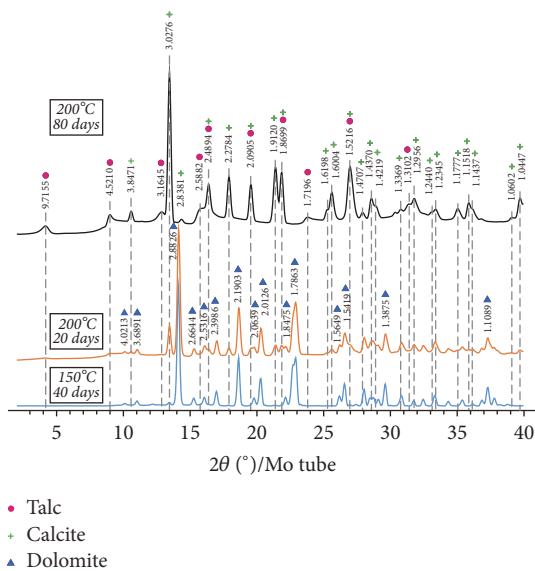


FIGURE 5: X-ray patterns of the solid relicts in FSCCs containing dolomite and water after heating at  $150^\circ\text{C}$  for  $\sim 40$  days (lower blue line) and at  $200^\circ\text{C}$  for  $\sim 20$  days (middle orange line) and  $\sim 80$  days (upper black line).

(e.g., [4–6]). However, serpentine minerals, like lizardite and chrysotile, are also likely to form at low temperatures during metamorphism of the  $\text{CaO-MgO-SiO}_2\text{-H}_2\text{O-CO}_2$  system, especially in contact or regional metamorphic settings [65–67]. Some researchers have even pointed out that serpentine forms at lower temperatures than talc during metamorphism

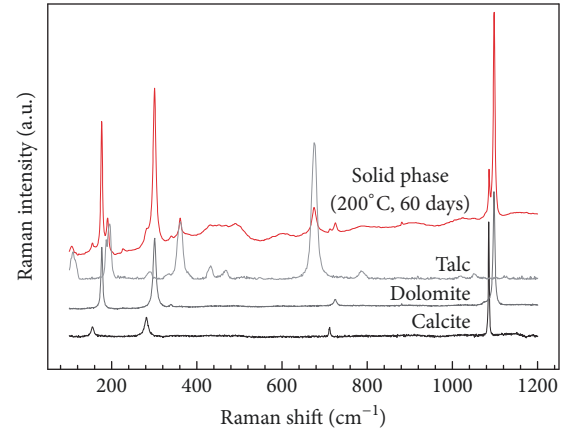


FIGURE 6: Raman spectrum of solid relicts after heating at  $200^\circ\text{C}$  for 60 days. The reference spectra of dolomite, calcite, and talc were also shown for comparison. The dolomite spectrum was acquired from the sample before heating. The calcite spectrum was acquired from crystalline calcite, and the reference spectrum of talc was cited from an open database hosted by the Department of Geosciences at the University of Arizona (RRUFF Project, <http://rruff.info/index.php>).

TABLE 2: Variations in the internal pressures of the HPOC containing dolomite and water with experimental duration at  $200^\circ\text{C}$ .

$t$ (h)	$P$ (psi)
0	209
3	221
6.3	224
9.2	223
12.2	224
22.2	210
25	215
28.5	215
32.5	215
34.6	216
46.3	217
49.2	217
52.9	219
58.9	219
70.4	221
73.6	221
76.8	223
79.7	224
82.9	227
94.3	222
97.3	212
99.9	218
107.5	206
127.6	208

of the  $\text{MgO-SiO}_2\text{-H}_2\text{O-CO}_2$  system [68, 69]. In fact, while serpentine is likely to form in a low-silica environment,

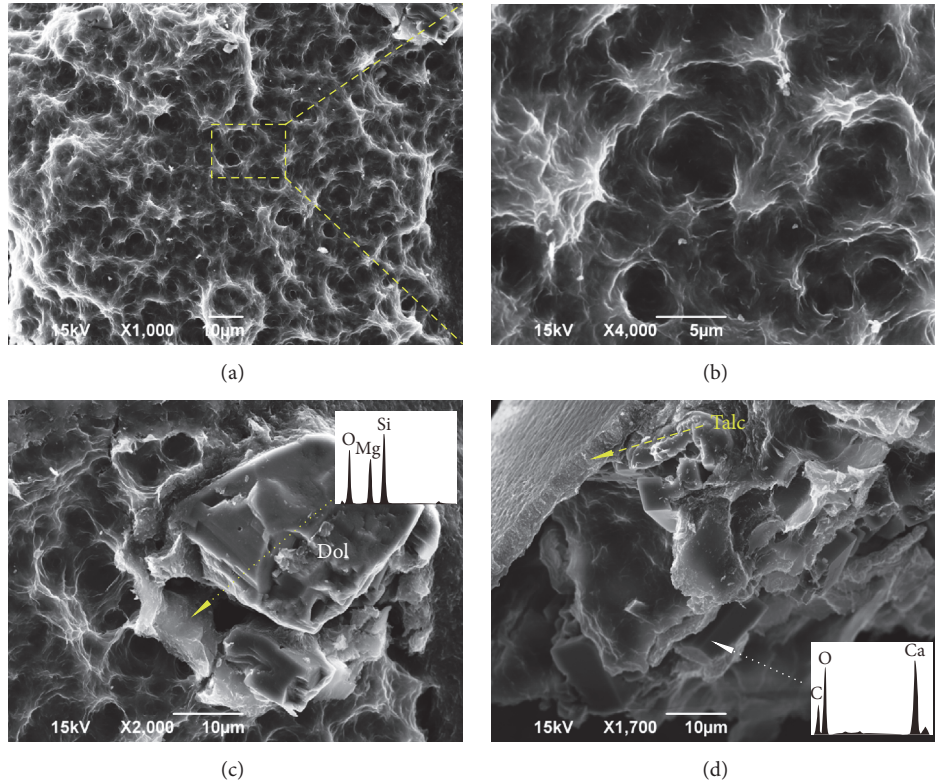


FIGURE 7: SEM micrographs and EDS analyses of the solid relicts in an FSCC containing dolomite and water after heating at 200°C for ~60 days. (a, b) Honeycomb-like talc; (c) dolomite grains with smooth edges and EDS result of talc (yellow arrow); (d) euhedral calcite formed in the relicts (white arrow) and cylindrical talc growing on the inner surface of the tube (yellow arrow).

further introduction of  $\text{SiO}_2$  will make talc stable relative to serpentine [70–73]. Considering the fact that talc was characterized as the product of Mg-silicate mineral in the 200°C experiment via reaction (1), we speculate that, while not detected by XRD, talc also formed below 200°C since  $\text{CO}_2$  was generated during the experiment (see above).

**3.3. Thermodynamic Calculations.** Due to the limits of the Unitherm database, we used aqueous silica as the  $\text{SiO}_2$  species that participated in the reaction. Considering that the solubility of amorphous silica was high at elevated temperatures [74], the calculated results should approximate the conditions of the experiments. The Gibbs free energy ( $\Delta G$ ) of formation for talc from  $\text{CaMg}(\text{CO}_3)_2$ , aqueous  $\text{SiO}_2$ , and  $\text{H}_2\text{O}$  at the pressure and temperature of interest are given in Table 3. The  $\Delta G$  of reaction decreases with increasing temperature at the saturation pressure. This indicates that the reaction is more favorable at higher temperatures. The  $\Delta G$  becomes negative at  $T \geq 80^\circ\text{C}$ , which implies that the formation of product talc from dolomite and a silica-rich fluid is thermodynamically favored. However, this reaction may not commence until even higher temperatures are reached due to the probable initial kinetic barrier to the reaction. These thermodynamic calculations support the implication from the experimental results that talc formation can occur at temperatures above 100°C.

## 4. Discussion

**4.1. Implications for the Formation of Mg-Carbonate-Hosted Talc.** Geologically, Prochaska [18] grouped the talc deposits into five types: (1) talc related to ultramafics (e.g., [13–15]); (2) Mg-carbonate-hosted talc (e.g., [20, 37]); (3) metamorphic talc (e.g., [75, 76]); (4) talc related to banded iron formations (mostly minnesotaite; [77, 78]); and (5) secondary talc deposits [18]. The most economically viable of these deposits are usually related to the metamorphic reaction between an Mg-carbonate infiltrated by a silica-rich hydrothermal fluid [18, 20, 21, 37]. Intense fractures that increase the permeability of geological fluid flow generally develop near such deposits [18, 20, 21, 37, 38].

Investigating the formation temperature of talc can improve our understanding of its mineralization process. This has previously been done using several methods. These include microthermometric measurements of relevant fluid inclusions (e.g., [39, 40, 79]) and calculations using talc–dolomite oxygen isotope thermometry, assuming that the mineral pairs achieve oxygen isotope equilibrium [21, 36]. In addition, the phase diagram of the  $\text{CaO-MgO-SiO}_2\text{-CO}_2\text{-H}_2\text{O}$  system has often been referred to for evaluating the formation temperature of talc [5, 35]. The diagram was established based on hydrothermal experiments, geological case studies, and thermodynamic calculations [4, 5, 43, 44]. However, the

TABLE 3: The Gibbs free energies of the reaction  $3\text{CaMg}(\text{CO}_3)_2 + 4\text{SiO}_2(\text{aq}) + \text{H}_2\text{O} = \text{Mg}_3(\text{Si}_4\text{O}_{10})(\text{OH})_2 + 3\text{CaCO}_3 + 3\text{CO}_2$  at the temperatures of interest and their corresponding saturation pressures.

Temperature ( $^{\circ}\text{C}$ )	$\Delta G^{\text{a}}$ (kJ/mol)	$P_{\text{sat}}^{\text{b}}$ (bar)	Temperature ( $^{\circ}\text{C}$ )	$\Delta G$ (kJ/mol)	$P_{\text{sat}}$ (bar)
25	7.709	0.032	100	-7.083	1.014
50	4.663	0.124	110	-9.951	1.434
60	2.771	0.199	120	-12.938	1.987
70	0.609	0.312	130	-16.032	2.703
80	-1.778	0.474	140	-19.223	3.615
90	-4.351	0.702	150	-22.502	4.761

<sup>a</sup> $\Delta G$  refers to the Gibbs free energy of the reaction; <sup>b</sup> $P_{\text{sat}}$  represents the corresponding saturation pressures, which are calculated based on the thermodynamic model proposed by Zhang and Duan [45].

experiments used to chart out this system have been generally conducted at  $>250^{\circ}\text{C}$  [4, 41–44]. The reaction path of the phase diagram at low temperatures was mainly established through thermodynamic calculations implying the need for talc forming experiments at temperatures below  $250^{\circ}\text{C}$ .

Some geological case studies attribute low talc mineralization temperatures ( $<200^{\circ}\text{C}$ ) derived from adjacent talc and dolomite oxygen isotope thermometry, to actually reflect isotopic disequilibrium [36]. This study shows that talc deposits can still form at temperatures below  $200^{\circ}\text{C}$  on geological time scales, especially if the product  $\text{CO}_2$  can be released (cf. reaction (1)). However, large-scale talc mineralization is more likely to form at higher temperatures (e.g.,  $250\text{--}400^{\circ}\text{C}$ ). Firstly,  $P_{\text{CO}_2}$  controls the lower thermal limit of talc stability. The onset temperature of the transformation increases with increasing  $P_{\text{CO}_2}$ , because  $\text{CO}_2$  is a product of the metamorphic reaction (1) and its presence greatly decreases the solubility of  $\text{SiO}_2$  in the fluid [80].  $\text{CO}_2$  is a common component in geological fluids and can be either released from magmas (e.g., [81–84]) or generated from the hydrothermal alteration of carbonate (e.g., [85–87]). The oxidation (e.g., [88]) and hydrothermal maturation of organic matter are also natural sources of  $\text{CO}_2$  [89, 90]. Therefore, talc mineralization should occur at relatively high temperatures in the presence of  $\text{CO}_2$ . Secondly, as our results have shown, the reaction rate for reaction (1) increases sharply with increasing temperature, facilitating talc deposits to form at higher temperatures.

This study can also contribute to understanding the fault weakening mechanism in the upper crust. The elastic strain accumulation along a fault can be released through a sudden seismic slip (earthquake) or aseismic creep slip [32]. A lower frictional coefficient for a fault will facilitate stable creep, weakening the fault and suppressing the occurrence of strong earthquakes [35]. The frictional coefficient of a fault generally decreases with increasing temperature [35]. Therefore, faults are likely to be weakened due to high temperatures in the deep crust, but not in the cool shallow crust. The pervasive distribution of clay minerals along faults has also been thought to weaken faults [33–35, 91–94], because layered clay minerals exhibit much lower frictional coefficients than other minerals [95]. For example, talc discovered along the San Andreas fault zone is responsible for helping in aiding slippage along the fault [35, 95]. As shown here, dolomite could react at  $\leq 200^{\circ}\text{C}$  with silica-rich fluids traveling along fault planes to form

talc and hence might be an important mechanism of fault weakening in carbonate sequences in the upper crust.

*4.2. Implications for Hydrothermal Dolomite Reservoir Research.* Carbonate rock is the main type of hydrocarbon reservoir worldwide, hosting over 60% of petroleum reserves [31]. Dolomite hydrocarbon reservoirs are important, comprising about half of the carbonate hydrocarbon reservoirs worldwide [96]. Recent research has suggested that hydrothermal alteration can increase the porosity and permeability of dolomite reservoirs substantially and is an important factor affecting the development and distribution of dolomite reservoirs [24, 25, 97–101]. The Tarim basin is one of the most important petroliferous basins in China and contains a lower Palaeozoic carbonate series, which is also an important hydrocarbon reservoir. Recent exploration has shown that silica-rich hydrothermal fluids have infiltrated these carbonate series, improving the physical properties of the reservoirs considerably (e.g., the Shunnan area of the Tarim Basin; [102, 103]). It has been proposed that silica-rich hydrothermal fluids were transported through extensional faults from the deep strata to the shallow carbonate sequence, where they migrated laterally through porous and permeable carbonate formations ( $\sim 6670$  m in the Shunnan area; [104]). Hydrothermal fluids originating in deep basins are generally hot. Microthermometric measurements have indicated that the silica-rich hydrothermal fluids in the Tarim basin reach over  $200^{\circ}\text{C}$  [101, 103]. Given that the lower part of the lower Palaeozoic sequence is mainly composed of dolomite, silica-rich hydrothermal fluids could react with the dolomite to form talc and thus change the physical properties of the reservoir. Recently, petrologic and diagenetic research have revealed pervasive silicification in Early Cretaceous ultra-deep water carbonate reservoirs in the Atlantic Ocean, offshore from Brazil [105]. The presence of talc, calcite, quartz, and dolomite on the thin-section scale may indicate that the dolomite was strongly corroded by a silica-rich hydrothermal fluid.

Alteration of dolomite to talc will also modify the porosity and permeability of carbonate hydrocarbon reservoirs [29–31]. The silica required for the mineral alteration can be provided by either silica-rich hydrothermal fluids or silica (e.g., quartz, chert, and opal) within the carbonate reservoirs [106]. If  $\text{SiO}_2$  derives from quartz/chert in the dolomite sequences,



the hydrothermal alteration would increase the porosity of the dolomite reservoirs. McKinley et al. [29] reported that the total volume of minerals within a dolomite reservoir can be reduced by 13% to 17% through the reaction between dolomite and quartz in reaction (1). In addition, the reaction between dolomite and silica-rich hydrothermal fluids can act as an important source of CO<sub>2</sub> in hydrocarbon reservoirs. The presence of CO<sub>2</sub> can lower the pH of the formation water and thus promote the dissolution of carbonate minerals [60, 107, 108], increasing the porosity of the reservoirs [109–111]. However, the pore throats may be blocked by the formation of talc or other clay minerals [29, 112]. Therefore, more detailed factors should be considered in order to unequivocally evaluate the effects of silica-rich hydrothermal fluids in dolomite reservoirs.

Although talc can form from the interaction between dolomite and silica-rich fluids at low temperatures, it is seldom observed in hydrocarbon reservoirs [29, 31] for the following two reasons. (1) A large amount of CO<sub>2</sub> can be produced by the maturation of organic matter and the reaction between carbonate minerals and organic acid [98, 101]. The presence of CO<sub>2</sub> decreases the lower thermal stability field of talc [113]. (2) The reaction path is dependent on the composition of the hydrothermal fluid. For example, K<sup>+</sup> and Al<sup>3+</sup> are also important components of geological fluids. Montmorillonite instead of talc is more likely to form in the presence of only a small quantity of Al<sup>3+</sup> [41], and the formation of talc can also be inhibited by K<sup>+</sup> [29].

**4.3. Implications for High P–T Experiment Using Fused Silica Capillary Tubes as Reactors.** FSCCs are used to construct synthetic fluid inclusions containing organic and inorganic components [46]. They offer advantages such as being inert to many components, especially acids and S, allowing for the convenient synthesis of fluid inclusions, and facilitating in situ optical and Raman spectroscopic observations (e.g., [57, 114–117]). Fused silica tubes can tolerate relatively high temperatures up to 600°C and pressures up to 300 MPa. As a result, FSCCs are used in many research fields. For example, in addition to construction of synthetic fluid inclusions [46, 53, 118], FSCCs were used in studying the properties of hydrothermal fluids as optical and Raman spectroscopic cells [115–117, 119–121]. FSCCs were also used as reactors in investigating the mechanism of thermochemical sulfate reduction [114] and the decomposition of organic matter [57].

However, SiO<sub>2</sub> in the FSCC acted as a reagent in this study and was partially dissolved, as indicated by the pits on the inner surface of the tube (Figures 8(a)–8(d)). The dissolution of silica from FSCCs containing alkali sulfate solutions was also observed after quenching from ≥350°C (Figures 8(e) and 8(f)). The severe dissolution of fused silica can be ascribed to three factors. (1) Amorphous silica is more soluble than quartz, especially at high temperatures. In neutral solutions, its solubility increases sharply with temperature from 100 ppm at 20°C to 1500 ppm at 310°C [74, 122, 123]. (2) Under basic conditions, the solubility of amorphous silica is greatly enhanced by the ionization of silicic acid ( $\text{H}_4\text{SiO}_4 + \text{OH}^- \rightarrow \text{H}_3\text{SiO}_4^- + \text{H}_2\text{O}$ ; [124]). (3)

SiO<sub>2</sub> may act as a reagent as it did in this experiment. The presence of dissolution pits will weaken the mechanical strength of the silica tube. In addition, the presence of dissolved silica can make the system more complicated than expected. Therefore, the solubility and reactivity of silica under hydrothermal conditions should be evaluated before FSCCs are used as reactors.

## 5. Conclusion

The reactions in the CaMg(CO<sub>3</sub>)<sub>2</sub>–SiO<sub>2</sub>–H<sub>2</sub>O system at low temperatures were investigated using fused silica tubes as reactors. Results showed that dolomite reacted with a silica-rich fluid to form talc, calcite, and CO<sub>2</sub> at ≤200°C and low P<sub>CO<sub>2</sub></sub>. The reaction rate increased with increasing temperature and decreased with rising P<sub>CO<sub>2</sub></sub>. Therefore, high temperature and the presence of a conduit to release CO<sub>2</sub> will promote the formation of talc. This experiment has important geological and geochemical implications.

(1) The results confirmed the mechanism of talc mineralization in Mg-carbonate hosted talc deposits. Dolomite reacted with silica-rich hydrothermal fluids to form talc, calcite, and CO<sub>2</sub>. Talc could form at ≤200°C, whereas previous hydrothermal experiments examining the CaO–MgO–SiO<sub>2</sub>–CO<sub>2</sub>–H<sub>2</sub>O system were mainly conducted at >250°C. However, considering the effect of temperature on the reaction rate, and other geological conditions, massive talc deposits are still more likely to form at higher temperatures. The formation of talc along a fault in a Mg-carbonate formation will also weaken the fault, thus preventing strong earthquakes.

(2) Talc in carbonate reservoirs can indicate the activity of silica-rich hydrothermal fluids. Fluid-aided alteration of dolomite can change the physical properties of dolomite reservoirs substantially. The reaction between dolomite and quartz within the carbonate can decrease the total volume of minerals by 13%–17%. The generation of CO<sub>2</sub> can promote the dissolution of carbonate minerals elsewhere under the appropriate conditions, increasing the porosity and permeability of carbonate reservoirs. However, talc minerals may block pore throats in the reservoirs. Therefore, additional factors need to be considered when evaluating the effects of CaMg(CO<sub>3</sub>)<sub>2</sub>–SiO<sub>2</sub>–H<sub>2</sub>O interactions on the physical properties of carbonate reservoirs.

(3) The solubility and reactivity of silica should be considered when using fused silica tubes as reactors in high P–T experiments. The dissolution of silica will increase the complexity of the system and weaken the mechanical strength of the tube.

## Conflicts of Interest

The authors declare that they have no conflicts of interest.

## Acknowledgments

The dolomite sample was provided by Mr. Chunhua Shi. Misses Yang Qu, Wanlu Gao, and Ye Qiu helped the authors a lot during the micro-XRD analysis and HPOC experiment.

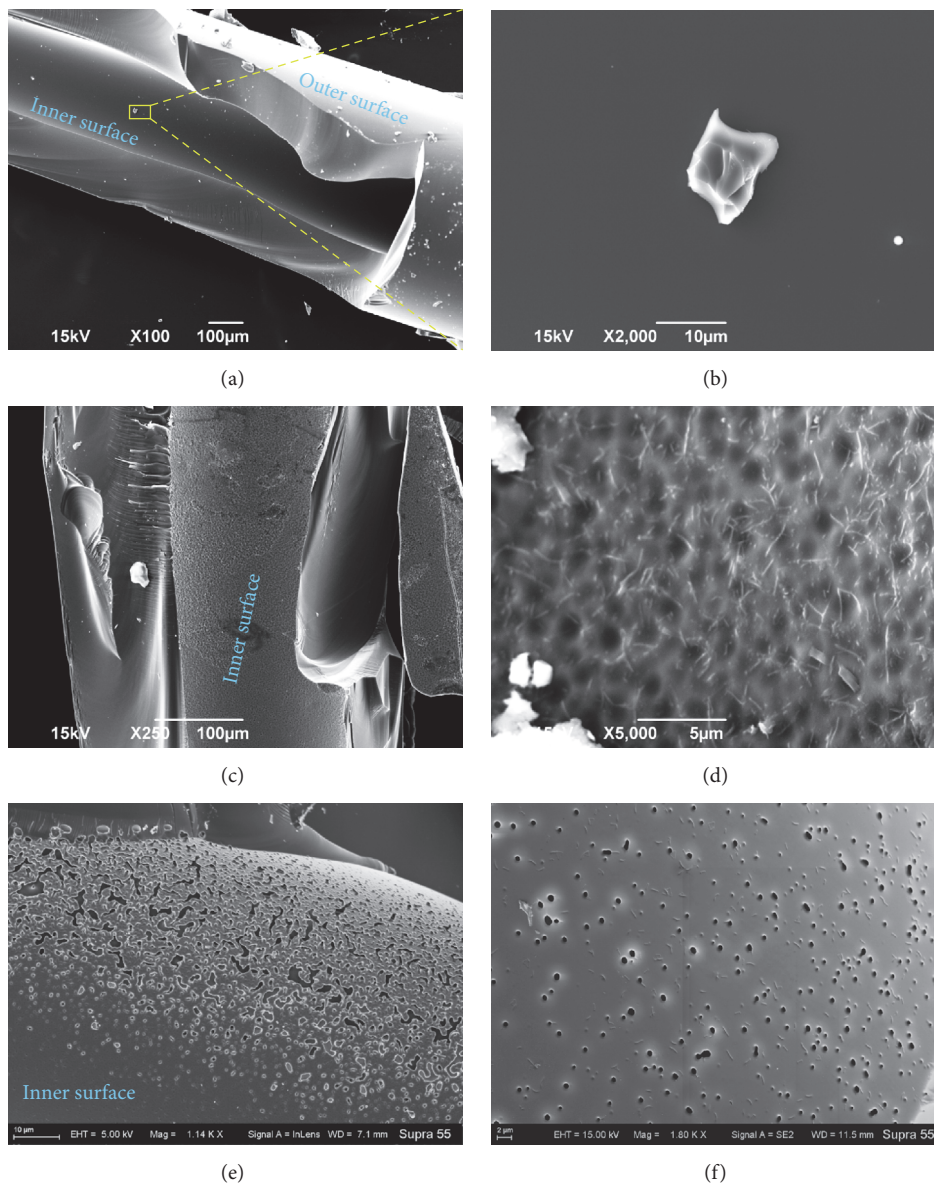


FIGURE 8: SEM images of the inner surface of the silica tube. (a) Smooth inner surface before the reaction; (b) magnification of the square area shown in (a); (c) dissolution pits on the inner surface after heating at 200°C for ~60 days; (d) magnification of (c); severe erosion of the silica on the inner surface of FSSCs containing (e) 1.0 m Na<sub>2</sub>SO<sub>4</sub> and (f) 1.0 m Li<sub>2</sub>SO<sub>4</sub> after heating at 350°C for 1 h.

Dr. Rui Wang and Miss Siyu Hu are also thanked for their help in the thermodynamic calculations of the reactions. This work was financially supported by the National Natural Science Foundation of China (Grant nos. 41230312 and 41573054). I-Ming Chou is thankful for the support of the Knowledge Innovation Program (SIDSSE-201302) and the Hadal-trench Research Program (XDB06060100) of Chinese Academy of Sciences.

## References

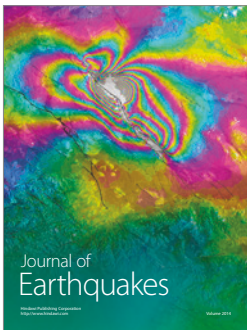
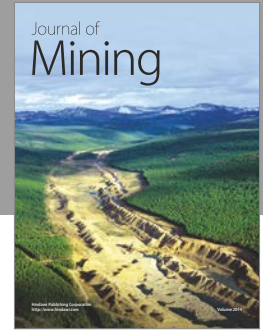
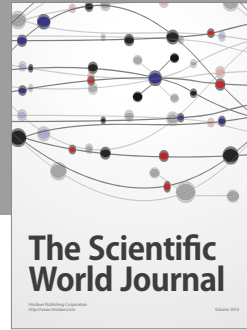
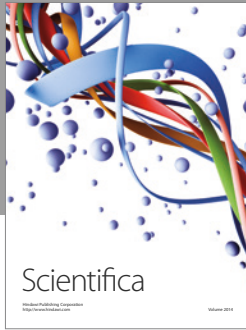
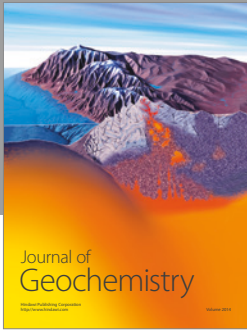
- [1] L. D. Meinert, "Skarns and skarn deposits," *Geoscience Canada*, vol. 19, no. 4, pp. 145–162, 1992.
- [2] L. D. Meinert, G. M. Dipple, and S. Nicolescu, "World skarn deposits," *Economic Geology 100th Anniversary Volume*, pp. 299–336, 2005.
- [3] Y. Yao, J. Chen, J. Lu, R. Wang, and R. Zhang, "Geology and genesis of the Hehuaping magnesian skarn-type cassiterite-sulfide deposit, Hunan Province, Southern China," *Ore Geology Reviews*, vol. 58, no. C, pp. 163–184, 2014.
- [4] T. M. Gordon and H. J. Greenwood, "The reaction dolomite + quartz + water = talc + calcite + carbon dioxide," *American Journal of Science*, vol. 268, pp. 225–242, 1970.
- [5] M. B. Holness, "Fluid flow paths and mechanisms of fluid infiltration in carbonates during contact metamorphism: The Beinn an Dubhaich aureole, Skye," *Journal of Metamorphic Geology*, vol. 15, no. 1, pp. 59–70, 1997.

- [6] W. Heinrich, S. S. Churakov, and M. Gottschalk, "Mineral-fluid equilibria in the system  $\text{CaO-MgO-SiO}_2\text{-H}_2\text{O-CO}_2\text{-NaCl}$  and the record of reactive fluid flow in contact metamorphic aureoles," *Contributions to Mineralogy and Petrology*, vol. 148, no. 2, pp. 131–149, 2004.
- [7] M. Wesolowski, "Thermal decomposition of talc: a review," *Thermochimica Acta*, vol. 78, no. 1-3, pp. 395–421, 1984.
- [8] L. A. Pérez-Maqueda, A. Duran, and J. L. Pérez-Rodríguez, "Preparation of submicron talc particles by sonication," *Applied Clay Science*, vol. 28, no. 1-4, pp. 245–255, 2005.
- [9] R. L. Johnson, "Talc," *American Ceramic Society Bulletin*, vol. 71, pp. 818–820, 1992.
- [10] R. L. Johnson and R. L. Virta, "Talc," *American Ceramic Society Bulletin*, vol. 79, pp. 79–81, 2000.
- [11] M. Z. Abzalov, "Chrome-spinels in gabbro-wehrlite intrusions of the Pechenga area, Kola Peninsula, Russia: emphasis on alteration features," *Lithos*, vol. 43, no. 3, pp. 109–134, 1998.
- [12] M. F. El-Sharkawy, "Talc mineralization of ultramafic affinity in the Eastern Desert of Egypt," *Mineralium Deposita*, vol. 35, no. 4, pp. 346–363, 2000.
- [13] M. Franceschelli, G. Carcangiu, A. M. Caredda, G. Cruciani, I. Memmi, and M. Zucca, "Transformation of cumulate mafic rocks to granulite and re-equilibration in amphibolite and greenschist facies in NE Sardinia, Italy," *Lithos*, vol. 63, no. 1-2, pp. 1–18, 2002.
- [14] S. G. Tesalina, P. Nimis, T. Augé, and V. V. Zaykov, "Origin of chromite in mafic-ultramafic-hosted hydrothermal massive sulfides from the Main Uralian Fault, South Urals, Russia," *Lithos*, vol. 70, no. 1-2, pp. 39–59, 2003.
- [15] D. M. Evans, "Metamorphic modifications of the Muremera mafic-ultramafic intrusions, eastern Burundi, and their effect on chromite compositions," *Journal of African Earth Sciences*, vol. 101, pp. 19–34, 2015.
- [16] T. Yamanaka, K. Maeto, H. Akashi et al., "Shallow submarine hydrothermal activity with significant contribution of magmatic water producing talc chimneys in the Wakamiko Crater of Kagoshima Bay, southern Kyushu, Japan," *Journal of Volcanology and Geothermal Research*, vol. 258, pp. 74–84, 2013.
- [17] B. Moine, J. P. Fortune, P. Moreau, and F. Viguier, "Comparative mineralogy, geochemistry, and conditions of formation of two metasomatic talc and chlorite deposits: Trimouns, Pyrenees, France, and Rabenwald, eastern Alps, Austria," *Economic Geology*, vol. 84, no. 5, pp. 1398–1416, 1989.
- [18] W. Prochaska, "Geochemistry and genesis of Austrian talc deposits," *Applied Geochemistry*, vol. 4, no. 5, pp. 511–525, 1989.
- [19] P. de Parseval, S. Jiang, F. Fontan, R. Wang, F. Martin, and J. Freet, "Geology and ore genesis of the Trimouns talc-chlorite ore deposit, Pyrénées, France," *Acta Petrologica Sinica*, vol. 20, no. 4, pp. 877–886, 2004.
- [20] A. C. Gondim and S. Jiang, "Geologic characteristics and genetic models for the talc deposits in Paraná and Bahia, Brazil," *Acta Petrologica Sinica*, vol. 20, no. 4, pp. 829–836, 2004.
- [21] P. Boulvais, P. de Parseval, A. D'Hulst, and P. Paris, "Carbonate alteration associated with talc-chlorite mineralization in the eastern Pyrenees, with emphasis on the St. Barthelemy Massif," *Mineralogy and Petrology*, vol. 88, no. 3-4, pp. 499–526, 2006.
- [22] G. R. Davies and L. B. Smith Jr., "Structurally controlled hydrothermal dolomite reservoir facies: an overview," *AAPG Bulletin*, vol. 90, no. 11, pp. 1641–1690, 2006.
- [23] J. Lonnee and H. G. Machel, "Pervasive dolomitization with subsequent hydrothermal alteration in the Clarke Lake gas field, Middle Devonian Slave Point Formation, British Columbia, Canada," *AAPG Bulletin*, vol. 90, no. 11, pp. 1739–1761, 2006.
- [24] J. A. Luczaj, "Evidence against the Dorag (mixing-zone) model for dolomitization along the Wisconsin arch - A case for hydrothermal diagenesis," *AAPG Bulletin*, vol. 90, no. 11, pp. 1719–1738, 2006.
- [25] L. B. Smith Jr., "Origin and reservoir characteristics of Upper Ordovician Trenton-Black River hydrothermal dolomite reservoirs in New York," *AAPG Bulletin*, vol. 90, no. 11, pp. 1691–1718, 2006.
- [26] J. Parnell, "Devonian Magadi-type cherts in the Orcadian Basin, Scotland," *Journal of Sedimentary Petrology*, vol. 56, no. 4, pp. 495–500, 1986.
- [27] J. M. García-Ruiz, "Carbonate precipitation into alkaline silica-rich environments," *Geology*, vol. 26, no. 9, pp. 843–846, 1998.
- [28] J. Zhang, W. Hu, Y. Qian et al., "Formation of saddle dolomites in Upper Cambrian carbonates, western Tarim Basin (northwest China): implications for fault-related fluid flow," *Marine and Petroleum Geology*, vol. 26, no. 8, pp. 1428–1440, 2009.
- [29] J. M. McKinley, R. H. Worden, and A. H. Ruffell, "Contact diagenesis: the effect of an intrusion on reservoir quality in the triassic sherwood sandstone group, Northern Ireland," *Journal of Sedimentary Research*, vol. 71, no. 3, pp. 484–495, 2001.
- [30] S. Dong, D. Chen, H. Qing et al., "Hydrothermal alteration of dolostones in the Lower Ordovician, Tarim Basin, NW China: multiple constraints from petrology, isotope geochemistry and fluid inclusion microthermometry," *Marine and Petroleum Geology*, vol. 46, pp. 270–286, 2013.
- [31] V. Madrucci, C. W. D. D. Anjos, R. A. Spadini, D. B. Alves, and S. M. C. Anjos, "Authigenic magnesian clays in carbonate reservoirs in Brazil," in *Proceedings of the 15th International Clay Conference*, Rio De Janeiro, Brazil, 2013.
- [32] C. H. Scholz, "Earthquakes and friction laws," *Nature*, vol. 391, no. 6662, pp. 37–42, 1998.
- [33] A. M. Schleicher, B. A. Van Der Pluijm, J. G. Solum, and L. N. Warr, "Origin and significance of clay-coated fractures in mudrock fragments of the SAFOD borehole (Parkfield, California)," *Geophysical Research Letters*, vol. 33, no. 16, Article ID L16313, 2006.
- [34] A. M. Schleicher, B. A. van der Pluijm, and L. N. Warr, "Nano-coatings of clay and creep of the San Andreas fault at Parkfield, California," *Geology*, vol. 38, no. 7, pp. 667–670, 2010.
- [35] C. Collettini, C. Viti, S. A. F. Smith, and R. E. Holdsworth, "Development of interconnected talc networks and weakening of continental low-angle normal faults," *Geology*, vol. 37, no. 6, pp. 567–570, 2009.
- [36] F. Tornos and B. F. Spiro, "The geology and isotope geochemistry of the talc deposits of Puebla de Lillo (Cantabrian zone, northern Spain)," *Economic Geology*, vol. 95, no. 6, pp. 1277–1296, 2000.
- [37] L. Hecht, R. Freiberger, H. A. Gilg, G. Grundmann, and Y. A. Kostitsyn, "Rare earth element and isotope (C, O, Sr) characteristics of hydrothermal carbonates: genetic implications for dolomite-hosted talc mineralization at Gopfersgrun (Fichtelgebirge, Germany)," *Chemical Geology*, vol. 155, no. 1-2, pp. 115–130, 1999.
- [38] R. Sharma, P. Joshi, and P. D. Pant, "The role of fluids in the formation of talc deposits of Rema area, Kumaun Lesser Himalaya," *Journal of the Geological Society of India*, vol. 73, no. 2, pp. 237–248, 2009.

- [39] P. De Parseval, B. Moine, J. P. Fortuné, and J. Ferret, "Fluid-mineral interactions at the origin of the Trimouns talc and chlorite deposit (Pyrénées, France)," in *Current Research in Geology Applied to Ore Deposits*, P. Fenoll Hach-Ali, J. Torrez-Ruiz, and F. Gervilla, Eds., pp. 205–209, University of Granada, Granada, Granada, Spain, 1993.
- [40] M. C. Boiron, P. Boulvais, M. Cathelineau, D. Banks, N. Calvayrac, and G. Hubert, "Fluid circulation at the origin of the trimouns talc deposit (Pyrenees, France)," in *Proceedings of the 18th Meeting of European Current Research on Fluid Inclusions*, Siena, Italy, 2005.
- [41] P. Bayliss and A. A. Levhinson, "Low temperature hydrothermal synthesis from dolomite or calcite, quartz and kaolinite," *Clays and Clay Minerals*, vol. 19, no. 2, pp. 109–114, 1971.
- [42] G. Skippen, "An experimental model for low pressure metamorphism of siliceous dolomitic marble," *American Journal of Science*, vol. 274, no. 5, pp. 487–509, 1974.
- [43] J. Slaughter, D. M. Kerrick, and V. J. Wall, "Experimental and thermodynamic study of equilibria in the system  $\text{CaO-MgO-SiO}_2\text{-H}_2\text{O-CO}_2$ ," *American Journal of Science*, vol. 275, pp. 143–162, 1975.
- [44] R. G. Eggert and D. M. Kerrick, "Metamorphic equilibria in the siliceous dolomite system: 6 kbar experimental data and geologic implications," *Geochimica et Cosmochimica Acta*, vol. 45, no. 7, pp. 1039–1049, 1981.
- [45] Z. Zhang and Z. Duan, "Prediction of the PVT properties of water over wide range of temperatures and pressures from molecular dynamics simulation," *Physics of the Earth and Planetary Interiors*, vol. 149, no. 3–4, pp. 335–354, 2005.
- [46] I.-M. Chou, Y. Song, and R. C. Burruss, "A new method for synthesizing fluid inclusions in fused silica capillaries containing organic and inorganic material," *Geochimica et Cosmochimica Acta*, vol. 72, no. 21, pp. 5217–5231, 2008.
- [47] I.-M. Chou, R. C. Burruss, and W. J. Lu, "A new optical cell for spectroscopic studies of geologic fluids at pressures up to 100 MPa," in *Advances in High-Pressure Technology for Geophysical Applications*, J. Chen, Y. Wang, T. S. Duffy, G. Shen, and L. F. Dobrzhinetskaya, Eds., pp. 475–485, Elsevier, Amsterdam, Netherlands, 2005.
- [48] K. M. Rosso and R. J. Bodnar, "Microthermometric and Raman spectroscopic detection limits of  $\text{CO}_2$  in fluid inclusions and the Raman spectroscopic characterization of  $\text{CO}_2$ ," *Geochimica et Cosmochimica Acta*, vol. 59, no. 19, pp. 3961–3975, 1995.
- [49] H. M. Lamadrid, *Geochemistry of fluid-rock processes [Doctoral dissertation]*, Virginia Polytechnic Institute and State University, Blacksburg, VA, USA, 2016.
- [50] J. H. Parker, D. W. Feldman, and M. Ashkin, "Raman scattering by silicon and germanium," *Physical Review*, vol. 155, no. 3, pp. 712–714, 1967.
- [51] Y. V. Shvarov, "Algorithmization of the numeric equilibrium modeling of dynamic geochemical processes," *Geochemistry International*, vol. 37, no. 6, pp. 571–576, 1999.
- [52] R. B. Wright and C. H. Wang, "Density effect on the Fermi resonance in gaseous  $\text{CO}_2$  by Raman scattering," *The Journal of Chemical Physics*, vol. 58, no. 7, pp. 2893–2895, 1973.
- [53] X. Wang, I.-M. Chou, W. Hu, R. C. Burruss, Q. Sun, and Y. Song, "Raman spectroscopic measurements of  $\text{CO}_2$  density: experimental calibration with high-pressure optical cell (HPOC) and fused silica capillary capsule (FSCC) with application to fluid inclusion observations," *Geochimica et Cosmochimica Acta*, vol. 75, no. 14, pp. 4080–4093, 2011.
- [54] H. R. Gordon and T. K. McCubbin Jr., "The 2.8-micron bands of  $\text{CO}_2$ ," *Journal of Molecular Spectroscopy*, vol. 19, no. 1–4, pp. 137–154, 1966.
- [55] T. Azbej, M. J. Severs, B. G. Rusk, and R. J. Bodnar, "In situ quantitative analysis of individual  $\text{H}_2\text{O-CO}_2$  fluid inclusions by laser Raman spectroscopy," *Chemical Geology*, vol. 237, no. 3–4, pp. 255–263, 2007.
- [56] Y. Song, I. M. Chou, W. Hu, B. Robert, and W. Lu, " $\text{CO}_2$  density-raman shift relation derived from synthetic inclusions in fused silica capillaries and its application," *Acta Geologica Sinica (English Edition)*, vol. 83, pp. 932–938, 2009.
- [57] Z. Pan, I.-M. Chou, and R. C. Burruss, "Hydrolysis of polycarbonate in sub-critical water in fused silica capillary reactor with in situ Raman spectroscopy," *Green Chemistry*, vol. 11, no. 8, pp. 1105–1107, 2009.
- [58] M. L. Frezzotti, F. Tecce, and A. Casagli, "Raman spectroscopy for fluid inclusion analysis," *Journal of Geochemical Exploration*, vol. 112, pp. 1–20, 2012.
- [59] E. L. Shock and H. C. Helgeson, "Calculation of the thermodynamic and transport properties of aqueous species at high pressures and temperatures: correlation algorithms for ionic species and equation of state predictions to 5 kb and 1000°C," *Geochimica et Cosmochimica Acta*, vol. 52, no. 8, pp. 2009–2036, 1988.
- [60] O. S. Pokrovsky, S. V. Golubev, J. Schott, and A. Castillo, "Calcite, dolomite and magnesite dissolution kinetics in aqueous solutions at acid to circumneutral pH, 25 to 150°C and 1 to 55 atm  $\text{pCO}_2$ : New constraints on  $\text{CO}_2$  sequestration in sedimentary basins," *Chemical Geology*, vol. 265, no. 1–2, pp. 20–32, 2009.
- [61] Y. Garrabos, R. Tufeu, B. Le Neindre, G. Zalczner, and D. Beysens, "Rayleigh and Raman scattering near the critical point of carbon dioxide," *The Journal of Chemical Physics*, vol. 72, no. 8, pp. 4637–4651, 1979.
- [62] J. H. Nicola, J. F. Scott, R. M. Couto, and M. M. Correa, "Raman spectra of dolomite [ $\text{CaMg}(\text{CO}_3)_2$ ]," *Physical Review B*, vol. 14, no. 10, pp. 4676–4678, 1976.
- [63] S. Gunasekaran, G. Anbalagan, and S. Pandi, "Raman and infrared spectra of carbonates of calcite structure," *Journal of Raman Spectroscopy*, vol. 37, no. 9, pp. 892–899, 2006.
- [64] G. J. Rosasco and J. J. Blaha, "Raman microprobe spectra and vibrational mode assignments of talc," *Applied Spectroscopy*, vol. 34, no. 2, pp. 140–144, 1980.
- [65] V. Trommsdorff and B. W. Evans, "Antigorite-ophicarbonates: phase relations in a portion of the system  $\text{CaO-MgO-SiO}_2\text{-H}_2\text{O-CO}_2$ ," *Contributions to Mineralogy and Petrology*, vol. 60, no. 1, pp. 39–56, 1977.
- [66] V. Trommsdorff and J. A. D. Connolly, "Constraints on phase diagram topology for the system  $\text{CaO-MgO-SiO}_2\text{-CO}_2\text{-H}_2\text{O}$ ," *Contributions to Mineralogy and Petrology*, vol. 104, no. 1, pp. 1–7, 1990.
- [67] B. S. Van Gosen, H. A. Lowers, S. J. Sutley, and C. A. Gent, "Using the geologic setting of talc deposits as an indicator of amphibole asbestos content," *Environmental Geology*, vol. 45, no. 7, pp. 920–939, 2004.
- [68] W. Johannes, "An experimental investigation of the system  $\text{MgO-SiO}_2\text{-H}_2\text{O-CO}_2$ ," *American Journal of Science*, vol. 267, no. 9, pp. 1083–1104, 1969.
- [69] E. S. Schandl and M. P. Gorton, "Hydrothermal alteration and  $\text{CO}_2$  metasomatism (natural carbon sequestration) of komatiites in the south-western Abitibi greenstone belt," *Canadian Mineralogist*, vol. 50, no. 1, pp. 129–146, 2012.

- [70] B. W. Evans and S. Guggenheim, "Talc, phyllosilicates, and related minerals," in *Reviews in Mineralogy*, S. W. Bailey, Ed., vol. 19, pp. 225–294, 1988.
- [71] B. Velde, "Experimental pseudomorphism of diopside by talc and serpentine in (Ni, Mg)Cl<sub>2</sub> aqueous solutions," *Geochimica et Cosmochimica Acta*, vol. 52, no. 2, pp. 415–424, 1988.
- [72] A. E. Williams-Jones, C. Normand, H. Clark Vali Jr., R. F. Martin, A. Dufresne, and Nayebzadeh A., "Controls of amphibole formation in chrysotile from the Jeffrey Mine, Asbestos Quebec," in *The Health Effects of Chrysotile Asbestos*, R. P. Nolan, A. M. Langer, M. Ross, Wicks F. J., and Martin F. R., Eds., vol. 5, pp. 89–104, The Mineralogical Association of Canada, Quebec, Canada, 2001.
- [73] B. W. Evans, "The serpentinite multisystem revisited: chrysotile is metastable," *International Geology Review*, vol. 46, no. 6, pp. 479–506, 2004.
- [74] I. Gunnarsson and S. Arnórsson, "Amorphous silica solubility and the thermodynamic properties of H<sub>4</sub>SiO<sub>4</sub> in the range of 0° to 350°C at P<sub>sat</sub>," *Geochimica et Cosmochimica Acta*, vol. 64, no. 13, pp. 2295–2307, 2000.
- [75] M. W. Bodine Jr., "Trioctahedral clay mineral assemblages in Paleozoic marine evaporite rocks," in *Proceedings of the Presented in the Sixth International Symposium on Salt*, vol. 1, pp. 267–284, Toronto, Canada, 1983.
- [76] W. Schreyer and K. Abraham, "Three-stage metamorphic history of a whiteschist from Sar e Sang, Afghanistan, as part of a former evaporite deposit," *Contributions to Mineralogy and Petrology*, vol. 59, no. 2, pp. 111–130, 1976.
- [77] T. Angerer and S. G. Hagemann, "The BIF-hosted high-grade iron ore deposits in the archaean koolyanobbing greenstone belt, Western Australia: structural control on synorogenic- and weathering-related magnetite-, hematite-, and goethite-rich iron ore," *Economic Geology*, vol. 105, no. 5, pp. 917–945, 2010.
- [78] P. Duuring and S. Hagemann, "Leaching of silica bands and concentration of magnetite in Archean BIF by hypogene fluids: Beebyn Fe ore deposit, Yilgarn Craton, Western Australia," *Mineralium Deposita*, vol. 48, no. 3, pp. 341–370, 2013.
- [79] D. Shin and I. Lee, "Fluid inclusions and their stable isotope geochemistry of the carbonate-hosted talc deposits near the Cretaceous Muamsa Granite, South Korea," *Geochemical Journal*, vol. 40, no. 1, pp. 69–85, 2006.
- [80] P. G. Novgorodov, "Solubility of quartz in an H<sub>2</sub>O–CO<sub>2</sub> mixture at 700 degrees C and pressures of 3 and 5 kbars," *Geokhimiya*, pp. 1484–1489, 1975.
- [81] T. M. Gerlach, "Chemical characteristics of the volcanic gases from Nyiragongo lava lake and the generation of CH<sub>4</sub>-rich fluid inclusions in alkaline rocks," *Journal of Volcanology & Geothermal Research*, vol. 8, no. 2–4, pp. 177–189, 1980.
- [82] J. V. Walther and P. M. Orville, "Volatile production and transport in regional metamorphism," *Contributions to Mineralogy and Petrology*, vol. 79, no. 3, pp. 252–257, 1982.
- [83] W. F. Giggenbach, "The origin and evolution of fluids in magmatic-hydrothermal systems," in *Geochemistry of Hydrothermal Ore Deposits*, H. L. Barnes, Ed., pp. 737–796, Wiley, New York, NY, USA, 3 edition, 1997.
- [84] J. B. Lowenstern, "Carbon dioxide in magmas and implications for hydrothermal systems," *Mineralium Deposita*, vol. 36, no. 6, pp. 490–502, 2001.
- [85] R. Kerrich and W. S. Fyfe, "The gold-carbonate association: source of CO<sub>2</sub>, and CO<sub>2</sub> fixation reactions in Archaean lode deposits," *Chemical Geology*, vol. 33, no. 1–4, pp. 265–294, 1981.
- [86] P. I. Nabelek, "Calc-silicate reactions and bedding-controlled isotopic exchange in the Notch Peak aureole, Utah: implications for differential fluid fluxes with metamorphic grade," *Journal of Metamorphic Geology*, vol. 20, no. 4, pp. 429–440, 2002.
- [87] P. I. Nabelek, "Fluid evolution and kinetics of metamorphic reactions in calc-silicate contact aureoles - From H<sub>2</sub>O to CO<sub>2</sub> and back," *Geology*, vol. 35, no. 10, pp. 927–930, 2007.
- [88] H. G. Machel, "Bacterial and thermochemical sulfate reduction in diagenetic settings - old and new insights," *Sedimentary Geology*, vol. 140, no. 1–2, pp. 143–175, 2001.
- [89] L. Stalker, P. Farrimond, and S. R. Larter, "Water as an oxygen source for the production of oxygenated compounds (including CO<sub>2</sub> precursors) during kerogen maturation," *Organic Geochemistry*, vol. 22, no. 3–5, pp. 477–IN4, 1994.
- [90] Z. K. Shipton, J. P. Evans, D. Kirschner, P. T. Kolesar, A. P. Williams, and J. Heath, "Analysis of CO<sub>2</sub> leakage through 'low-permeability' faults from natural reservoirs in the Colorado Plateau, east-central Utah," *Geological Society Special Publication*, vol. 233, pp. 43–58, 2004.
- [91] J. Byerlee, "Friction, overpressure and fault normal compression," *Geophysical Research Letters*, vol. 17, no. 12, pp. 2109–2112, 1990.
- [92] C. Morrow, B. Radney, and J. Byerlee, "Chapter 3 frictional strength and the effective pressure law of montmorillonite and illite clays," *International Geophysics*, vol. 51, no. C, pp. 69–88, 1992.
- [93] C. A. Morrow, D. E. Moore, and D. A. Lockner, "The effect of mineral bond strength and adsorbed water on fault gouge frictional strength," *Geophysical Research Letters*, vol. 27, no. 6, pp. 815–818, 2000.
- [94] D. A. Lockner, C. Morrow, D. Moore, and S. Hickman, "Low strength of deep San Andreas fault gouge from SAFOD core," *Nature*, vol. 472, no. 7341, pp. 82–86, 2011.
- [95] D. E. Moore and M. J. Rymer, "Talc-bearing serpentinite and the creeping section of the San Andreas fault," *Nature*, vol. 448, no. 7155, pp. 795–797, 2007.
- [96] D. H. Zenger, "Discussion: 'On the formation and occurrence of saddle dolomite,'" *Journal of Sedimentary Petrology*, vol. 51, no. 4, pp. 1350–1352, 1981.
- [97] D. A. Katz, G. P. Eberli, P. K. Swart, and L. B. Smith Jr., "Tectonic-hydrothermal brecciation associated with calcite precipitation and permeability destruction in Mississippian carbonate reservoirs, Montana and Wyoming," *AAPG Bulletin*, vol. 90, no. 11, pp. 1803–1841, 2006.
- [98] M. Esteban and C. Taberner, "Secondary porosity development during late burial in carbonate reservoirs as a result of mixing and/or cooling of brines," *Journal of Geochemical Exploration*, vol. 78–79, pp. 355–359, 2003.
- [99] H. G. MacHel, "Investigations of burial diagenesis in carbonate hydrocarbon reservoir rocks," *Geoscience Canada*, vol. 32, no. 3, pp. 103–128, 2005.
- [100] J. A. Sagan and B. S. Hart, "Three-dimensional seismic-based definition of fault-related porosity development: Trenton-Black River interval, Saybrook, Ohio," *AAPG Bulletin*, vol. 90, no. 11, pp. 1763–1785, 2006.
- [101] F. Xing and S. Li, "Genesis and environment characteristics of dolomite-hosted quartz and its significance for hydrocarbon exploration, in Keping Area, Tarim Basin, China," *Journal of Earth Science*, vol. 23, no. 4, pp. 476–489, 2012.
- [102] L. Yun and Z. Cao, "Hydrocarbon enrichment pattern and exploration potential of the Ordovician in Shunnan area, Tarim Basin," *Oil and Gas Geology*, vol. 35, no. 6, pp. 788–797, 2014.

- [103] Y. Li, N. Ye, X. Yuan, Q. Huang, B. Su, and R. Zhou, "Geological and geochemical characteristics of silicified hydrothermal fluids in Well Shunnan 4, Tarim Basin," *Oil and Gas Geology*, vol. 36, no. 6, pp. 934–944, 2015.
- [104] L. Qi, "Oil and gas breakthrough in ultra-deep Ordovician carbonate formations in Shuntuoguole uplift, Tarim Basin," *China Petroleum Exploration*, vol. 21, no. 3, pp. 38–51, 2016, (in Chinese with English abstract).
- [105] H. R. Qing, "An introduction of petrology and diagenesis of ultra-deep water carbonate reservoirs from the Atlantic Ocean, offshore Brazil," 2017, Oral presentation at Wuxi Institute of Petroleum Geology of SINOPEC, Wuxi, China.
- [106] G. J. Simandl and S. Paradisil, "Carbonate-hosted talc," *Selected British Columbia Mineral Deposit Profiles*, vol. 3, pp. 35–38, 1999.
- [107] Y. K. Kharaka, D. R. Cole, S. D. Hovorka, W. D. Gunter, K. G. Knauss, and B. M. Freifeld, "Gas-water-rock interactions in Frio Formation following CO<sub>2</sub> injection: implications for the storage of greenhouse gases in sedimentary basins," *Geology*, vol. 34, no. 7, pp. 577–580, 2006.
- [108] Z. Duan and D. Li, "Coupled phase and aqueous species equilibrium of the H<sub>2</sub>O–CO<sub>2</sub>–NaCl–CaCO<sub>3</sub> system from 0 to 250°C, 1 to 1000 bar with NaCl concentrations up to saturation of halite," *Geochimica et Cosmochimica Acta*, vol. 72, no. 20, pp. 5128–5145, 2008.
- [109] M. R. Giles and J. D. Marshall, "Constraints on the development of secondary porosity in the subsurface: re-evaluation of processes," *Marine and Petroleum Geology*, vol. 3, no. 3, pp. 243–255, 1986.
- [110] O. S. Pokrovsky, S. V. Golubev, and J. Schott, "Dissolution kinetics of calcite, dolomite and magnesite at 25°C and 0 to 50 atm pCO<sub>2</sub>," *Chemical Geology*, vol. 217, no. 3–4, pp. 239–255, 2005.
- [111] P. Cao, Z. T. Karpyn, and L. Li, "The role of host rock properties in determining potential CO<sub>2</sub> migration pathways," *International Journal of Greenhouse Gas Control*, vol. 45, pp. 18–26, 2016.
- [112] M. D. Fishburn, "Significant results of deep drilling at Elk Hills, Kern County, California," in *Structure, Stratigraphy and Hydrocarbon Occurrences of the San Joaquin Basin, California*, G. K. Kuespert and S. A. Reid, Eds., vol. 64, pp. 157–167, Pacific Sections, Society of Economic Paleontologists and Mineralogists and American Association of Petroleum Geologists, 1990.
- [113] E. Povoden, M. Horacek, and R. Abart, "Contact metamorphism of siliceous dolomite and impure limestones from the Werfen formation in the eastern Monzoni contact aureole," *Mineralogy and Petrology*, vol. 76, no. 1–2, pp. 99–120, 2002.
- [114] S. Yuan, I.-M. Chou, R. C. Burruss, X. Wang, and J. Li, "Disproportionation and thermochemical sulfate reduction reactions in S–H<sub>2</sub>O–CH<sub>4</sub> and S–D<sub>2</sub>O–CH<sub>4</sub> systems from 200 to 340°C at elevated pressures," *Geochimica et Cosmochimica Acta*, vol. 118, pp. 263–275, 2013.
- [115] X. Wang, I.-M. Chou, W. Hu, and R. C. Burruss, "In situ observations of liquid-liquid phase separation in aqueous MgSO<sub>4</sub> solutions: geological and geochemical implications," *Geochimica et Cosmochimica Acta*, vol. 103, pp. 1–10, 2013.
- [116] X. Wang, Y. Wan, W. Hu et al., "In situ observations of liquid-liquid phase separation in aqueous ZnSO<sub>4</sub> solutions at temperatures up to 400°C: Implications for Zn<sup>2+</sup>–SO<sub>4</sub><sup>2-</sup> association and evolution of submarine hydrothermal fluids," *Geochimica et Cosmochimica Acta*, vol. 181, pp. 126–143, 2016.
- [117] X. Wang, I.M. Chou, W. Hu, Y. Wan, and Z. Li, "Properties of lithium under hydrothermal conditions revealed by in situ Raman spectroscopic characterization of Li<sub>2</sub>O–SO<sub>3</sub>–H<sub>2</sub>O (D<sub>2</sub>O) systems at temperatures up to 420°C," *Chemical Geology*, vol. 451, pp. 104–115, 2017.
- [118] L. Shang, I.-M. Chou, W. Lu, R. C. Burruss, and Y. Zhang, "Determination of diffusion coefficients of hydrogen in fused silica between 296 and 523 K by Raman spectroscopy and application of fused silica capillaries in studying redox reactions," *Geochimica et Cosmochimica Acta*, vol. 73, no. 18, pp. 5435–5443, 2009.
- [119] M. Dargent, J. Dubessy, L. Truche, E. F. Bazarkina, C. Nguyen-Trung, and P. Robert, "Experimental study of uranyl(VI) chloride complex formation in acidic LiCl aqueous solutions under hydrothermal conditions ( $T = 21^{\circ}\text{C} - 350^{\circ}\text{C}$ , Psat) using Raman spectroscopy," *European Journal of Mineralogy*, vol. 25, no. 5, pp. 765–775, 2013.
- [120] Y. Wan, X. Wang, W. Hu, and I.-M. Chou, "Raman spectroscopic observations of the ion association between Mg<sup>2+</sup> and SO<sub>4</sub><sup>2-</sup> in MgSO<sub>4</sub>-saturated droplets at temperatures of  $\leq 380^{\circ}\text{C}$ ," *The Journal of Physical Chemistry A*, vol. 119, no. 34, pp. 9027–9036, 2015.
- [121] Y. Wan, X. Wang, W. Hu, I. M. Chou, Y. Chen, and Z. Xu, "In situ optical and Raman spectroscopic observations of the effects of pressure and fluid composition on liquid-liquid phase separation in aqueous cadmium sulfate solutions (=400°C, 50 MPa) with geological and geochemical implications," *Geochimica et Cosmochimica Acta*, vol. 211, pp. 133–152, 2017.
- [122] W. L. Marshall, "Amorphous silica solubilities—I. Behavior in aqueous sodium nitrate solutions; 25–300°C, 0–6 molal," *Geochimica et Cosmochimica Acta*, vol. 44, no. 7, pp. 907–913, 1980.
- [123] C.-T. A. Chen and W. L. Marshall, "Amorphous silica solubilities IV. Behavior in pure water and aqueous sodium chloride, sodium sulfate, magnesium chloride, and magnesium sulfate solutions up to 350°C," *Geochimica et Cosmochimica Acta*, vol. 46, no. 2, pp. 279–287, 1982.
- [124] B. A. Fleming and D. A. Crerar, "Silicic acid ionization and calculation of silica solubility at elevated temperature and pH application to geothermal fluid processing and reinjection," *Geothermics*, vol. 11, no. 1, pp. 15–29, 1982.



**Hindawi**

Submit your manuscripts at  
<https://www.hindawi.com>

